HHS Public Access

Author manuscript

Med Phys. Author manuscript; available in PMC 2021 September 16.

Published in final edited form as:

Med Phys. 2021 February ; 48(2): 715–723. doi:10.1002/mp.14643.

Mapping lung ventilation through stress maps derived from biomechanical models of the lung

Guillaume Cazoulat[a)]

Department of Imaging Physics, The University of Texas MD Anderson Cancer Center, Houston, TX, USA

James M. Balter, **Martha M. Matuszak**, **Shruti Jolly**, **Dawn Owen**

Department of Radiation Oncology, University of Michigan, Ann Arbor, MI, USA

Kristy K. Brock

Department of Imaging Physics, The University of Texas MD Anderson Cancer Center, Houston, TX, USA

Abstract

Purpose: Most existing computed tomography (CT)-ventilation imaging techniques are based on deformable image registration (DIR) of different respiratory phases of a four-dimensonal CT (4DCT) scan of the lung, followed by the quantification of local breathing-induced changes in Hounsfield Units (HU) or volume. To date, only moderate correlations have been reported between these CT-ventilation metrics and standard ventilation imaging modalities for adaptive lung radiation therapy. This study evaluates the use of stress maps derived from biomechanical model-based DIR as an alternative CT-ventilation metric.

Materials and methods: Six patients treated for lung cancer with conventional radiation therapy were retrospectively analyzed. For each patient, a 4DCT scan and Tc-99m SPECT-V image acquired for treatment planning were collected. Biomechanical model-based DIR was applied between the inhale and exhale phase of the 4DCT scans and stress maps were calculated. The voxel-wise correlation between the reference SPECT-V image and map of the maximum principal stress was measured with a Spearman correlation coefficient. The overlap between high (above the 75th percentile) and low (below the 25th percentile) functioning volumes extracted from the reference SPECT-V and the stress maps was measured with Dice similarity coefficients (DSC). The results were compared to those obtained when using two classical CT-ventilation metrics: the change in HU and Jacobian determinant.

Results: The mean Spearman correlation coefficients were: 0.37 ± 18 and 0.39 ± 13 and 0.59 ± 0.13 considering the changes in HU, Jacobian and maximum principal stress, respectively. The corresponding mean DSC coefficients were 0.38 ± 0.09, 0.37 ± 0.07 and 0.52 ± 0.07 for the high ventilation function volumes and 0.48 ± 0.13, 0.44 ± 0.09 and 0.52 ± 0.07 for the low ventilation function volumes.

[a)]Author to whom correspondence should be addressed. gcazoulat@mdanderson.org.

Conclusion: For presenting a significantly stronger and more consistent correlation with standard SPECT-V images than previously proposed CT-ventilation metrics, stress maps derived with the proposed method appear to be a promising tool for incorporation into functional lung avoidance strategies.

Keywords

biomechanics; CT-ventilation imaging; lung cancer

1. INTRODUCTION

Management of lung cancer includes radiation therapy for the majority of patients.[1] A common side-effect of lung radiotherapy, and a limiting factor for dose escalation trials, is radiation-induced pneumonitis.[2–6] To reduce the risk of toxicity, functional lung avoidance techniques have been proposed, consisting of taking into account the spatial heterogeneity of the lung function at planning into the optimization process of the dose distribution.[7,8] The definition of functional volumes for planning has typically relied on the acquisition of ventilation/perfusion single photon emission computed tomography (SPECT) scan in addition to the standard computed tomography (CT) scans acquired for treatment planning.[9]

Previous studies have suggested that the lung ventilation functional distribution could be derived from the planning CT scan alone, which would enable functional lung avoidance without increasing the burden for the patient and financial cost of the treatment protocol. This concept, named CT-ventilation imaging and used in three clinical US trials for functional lung avoidance (NCT02528942, NCT02308709, NCT0284356), mainly relies on the calculation of two metrics after deformable image registration (DIR) between different temporal phases of 4D CT scans typically acquired to assess the movement of tumors and/or other organs to assist target definition for patients treated while breathing freely. The first approach consisted of estimating the ventilation at each corresponding voxel in the lungs as a function of change in Hounsfield Units (HU).[10] A second approach focused on estimating the local ventilation by calculating the local volume change given by the determinant of the Jacobian of the displacement vector field (DVF).[11] Other studies have since reported correlation measures between CT-ventilation maps, derived by these or other methods, and reference lung function maps extracted from images such as SPECT ventilation/perfusion,[12–15] contrast-enhanced Xenon CT for sheep,[16,17] hyperpolarized magnetic resonance (MR)[18] or positron emission tomography (PET) using $^{68}GaCl_3$-labeled pseudogas (“Galligas”).[19] These studies have demonstrated a correlation between the CT-ventilation maps and reference images when considering the contribution of sub-volumes of the lung to the total ventilation function. However, in the studies that reported a voxel-wise correlation between the CT-ventilation maps and reference ventilation images, a weak and highly variable correlation was found for SPECT images[14,20] and at best was qualified as moderate for PET Galligas images.[19]

Among existing DIR strategies for CT scans of the lung, a method based on biomechanical modeling has previously been demonstrated to provide accurate displacement vector fields (DVF), especially in registering the exhale to the inhale phase of 4DCT scans.[21] This finite-

element model (FEM)-based method (Morfeus) has the additional advantage, compared to traditional DIR algorithms, of allowing the definition of heterogeneous elastic properties inside the lung while controlling local deformation based on image features, in this case the lung and vasculature segmentations. It has been demonstrated that this method provides an accurate estimation of the DVF, and therefore the strain distribution in the lung. Assuming that the local ventilation function is proportional to the local air-induced volume change, which can be measured directly by the strain given by DIR, and to the local density of normal lung tissue (which might be related to the elasticity), the stress, defined as the product of strain and elasticity, appears as a natural metric for this ventilation function. In this paper, we propose to expand the biomechanical model-based DIR method to calculate mechanical stress maps and evaluate their correlation with reference ventilation imaging.

Recently, the VAMPIRE Challenge was conducted, aiming to quantify the variability in proposed CT-ventilation maps based on different DIR methods and CT-ventilation metric as well as their correlation with three different reference ventilation image modalities: Xenon CT for sheep, DTPA-SPECT and Galligas 4DPET/CT for humans.[22] Considering stress maps as the CT-ventilation metric as an alternative to other proposed metrics yielded a substantially higher correlation with the reference imaging for the human datasets. This paper describes the method to generate the stress maps and provides further evaluation of the correlation with SPECT-V data from six additional patients not included in the VAMPIRE Challenge.

2. MATERIALS AND METHODS

2.A. Patient data

Six lung cancer patients who underwent SPECT-V scans as part of treatment on an IRB-approved adaptive radiation therapy protocol were retrospectively analyzed for this study. Each patient had a 4DCT scan for planning, reconstructed using 10 bins with axial spatial resolution ranging from 0.93 to 1.18 mm and consistent slice spacing of 3 mm. The inhale and exhale phases were selected by visually assessing which phases presented with the minimum and maximum lung inflation levels. Contours of the left and right lungs were manually delineated on both phases in the treatment planning system (Eclipse, Varian Medical Systems, Palo Alto, California, USA). For all patients, a ventilation Tc-99m SPECT (SPECT-V) scan of resolution $0.9 \times 0.9 \times 2$ mm was acquired prior to treatment and used for analysis.

2.B. Stress maps computation

The workflow of the biomechanical model-based deformable registration method (Morfeus) used for the lung is represented Fig. 1 and has previously been described in detail.[21] Briefly, it consists first of generating a tetrahedral mesh of the lung and body from the contours of the reference fixed image, in this case the inhale phase of the 4DCT. A surface projection algorithm was then used between the lung surfaces defined on the two images, based on the computation of distance maps from the lung contours followed by application of DIR with a variant of the Demons algorithm. The displacements estimated using the Demons algorithm were used to define boundary conditions in the FEM. Instead of applying displacements

directly on the lung surface nodes, the displacements were applied on the chest cavity nodes. Thanks to the definition of a frictionless contact surface between the lung and chest wall, this approach allowed to simulate the physiological lung sliding and to limit the impact of a possible inaccurate surface projection.[23] In parallel, vessels were automatically segmented in the two images and nonrigidly registered to define boundary conditions on their centerline. A numerical simulation of the displacement of all nodes of the mesh was finally performed using the finite-element analysis software Optistruct (Altair Engineering, Troy, MI).

The introduction of heterogeneous elastic properties in this workflow was demonstrated to have a negligible impact on the resulting DVF.[24] However, in order to accurately calculate the stress distribution, or the local resistance of the lung tissue to the deformation imposed by the boundary conditions, variations in elastic properties of the lung must be defined. A wide range of elastic properties were considered in previous work on finite-element modeling of the lung with a linear elastic model, with a Poisson's ratio ranging from 0.1 to 0.49 and a Young's modulus ranging from 0.1 to 7.8 kPa.[25–28] In this study, based on these orders of magnitude, the elements' compressibility was assumed constant with a Poisson's ratio set to 0.4 as in the previously proposed Morfeus workflow for DIR and variable Young's moduli (E) were assigned to different regions of the lung ranging from 1 kPa for the definition of air to a maximum of 20 kPa for the definition of the stiffest lung tissues such as fibrosis.

The assignment of different elastic properties in the FEM and the generation of stress maps are illustrated in Fig. 2. To estimate the Young's modulus spatial distribution, a linear relationship was assumed with the density of lung tissue given by the HU in the inhale CT scan. Voxels with HU below −950 were considered as air only and those with HU above −200 as the stiffest tissue. The stiffness in all other voxels was assumed linearly proportional to the corresponding HU. Each tetrahedral element of the lung was assigned a Young's modulus based on the density at the tetrahedron centroid location in the inhale CT. Since the tetrahedral mesh resolution (5 mm) was much coarser than the image, the inhale CT scan was first smoothed with a Gaussian filter of radius 6 mm to ensure a smooth distribution of the stiffness in the mesh. To obtain a single scalar value at the centroid coordinates $\boldsymbol{c_k}$ of each tetrahedron k of the mesh, the maximum principal stress σ_{k_1}, defined as the maximum eigenvalue of the Cauchy stress tensor $\boldsymbol{\sigma}_k$, was calculated using the finite-element analysis software Optistruct (Altair Engineering). The scattered σ_{k_1} distribution was then resampled on the grid of the reference image to generate a stress map V_{Stress} directly comparable to a reference ventilation function map.

2.C. SPECT-V and stress maps similarity analysis

The SPECT-V was aligned with the average CT generated from the planning DCT in the TPS Eclipse as performed for treatment planning. The same comparison was performed between the generated and reference ventilation images as in many CT-ventilation imaging studies, in particular the VAMPIRE challenge.[22]

First, the Spearman correlation coefficient was calculated between the generated stress maps and reference ventilation images in a mask defined by the contours of the lung in the exhale

image. This coefficient measures the strength of the monotonicity between the two-paired distributions.

Second, in order to compare the identification of high and low functioning volumes in the lung, thresholds were applied to the stress maps and SPECT-based ventilation maps based on the individual patient's map. For each patient's individual stress map and SPECT ventilation map, the low functioning volume included all lung voxels below the 25th percentile of the patient's specific map distribution and the high functioning volume all lung voxels above the 75th percentile. Dice similarity coefficients (DSC) were calculated between the high and low functional volumes extracted from the stress maps and the reference SPECT-V images. The patient-specific determination of the high and low functioning volumes of the lung is acceptable as the ventilation maps are used to assess relative lung function on individual patients (as opposed to the whole patient population).

2.D. Comparison with other methods

The similarity results obtained with the analysis of the V_{Stress} maps were compared to those obtained when considering the two other mainly used CT-ventilation metrics: the local volume change and local change in air density. The local volume change was measured by the Jacobian determinant J of the inverse of the DVF calculated from Morfeus, so that a local tissue expansion yielded J >1 and a local contraction J <1 as in Ref. [11]. The corresponding CT-ventilation map was noted V_{Jac}. The CT-ventilation map based on change in air density, noted V_{HU}, was also calculated using the inverse of the DVF from Morfeus and following the equation[19]:

$$V_{HU}(\boldsymbol{x}) = \frac{I_{ex}(\boldsymbol{x}) - I_{in}(\boldsymbol{x}+\boldsymbol{u})}{I_{in}(\boldsymbol{x}+\boldsymbol{u}) + 1000},$$

with I_{ex} and I_{in} respectively the exhale and inhale images and the displacement vector $\boldsymbol{u}$ at the corresponding voxel coordinates $\boldsymbol{x}$. For comparison of the results with previous studies, the V_{Jac} and V_{HU} maps were smoothed with a median filter of width 3 × 3 × 3 voxels.[22]

Statistical differences between the mean Spearman correlation coefficients and mean DSCs obtained with the different CT-ventilation methods were assessed with two-tailed paired *t*-tests.

3. RESULTS

3.A. Spearman correlation coefficients

Figure 3 shows the breathing motion magnitude for the six patients with a color overlay between coronal slices of the inhale and exhale phases of the 4DCT scans. For each patient, the following were also represented on the same coronal slice: the SPECT-V image, the computed stress map and a scatter plot of their relationship. For visualization purposes, the SPECT-V and stress images were normalized for each patient by linearly rescaling the 0–90th percentiles between 0 and 1 and by setting the visualization window/level to 1/0.5.

Various forms of ventilation function distributions were observed. Patient 1 did not present any particular ventilation defect, with the entire lung demonstrating breathing-induced motion. On the reference SPECT-V image, areas of high ventilation function could be observed near the direct exit of the main airways and the signal globally decreased with the distance to these areas of high ventilation. The stress map computed for this patient presented a similar pattern due to the higher stiffness defined around the main vasculature. The SPECT images for Patients 2 and 3 presented low ventilation function in the upper lobe of their right and left lung, respectively. These defects, which were likely due to an obstruction of the airflow by the tumor, could also be observed on the generated stress maps resulting from the low volume change (e.g. low strain) calculated in this area. Patient 4 was the case presenting the lowest correlation between SPECT-V and stress. It appeared that the imaging aerosol did not enter the right lung at the time of the SPECT acquisition whereas the 4DCT scan seemed to exhibit ventilation-induced volume change of the right middle and inferior lobes. However, the correlation for the left lobe alone appeared high. The highest Spearman correlation coefficients, above 0.7, were obtained for Patient 5 and 6 who both presented large regions with poor ventilation function. For Patient 5, the defect corresponded to the presence of emphysema in the upper part of the lungs while for Patient 6, the airways were obstructed preventing the air to enter the middle and upper lobe of the right lung.

Figure 4 reports the Spearman correlation coefficients measured between the three different CT-ventilation calculations and the SPECT-V intensity distribution. With a mean Spearman coefficient of 0.59 ± 0.13, the correlation between the stress maps and reference imaging was significantly higher ($P < 0.05$) than when considering the Jacobian (0.39 ± 13) or changes in HU (0.37 ± 18). The stress map provided the highest correlation with the SPECT-V ventilation map for all patients except Patient 4. We hypothesize that this difference could be due to an actual variation of the ventilation function between the time of the SPECT and planning 4DCT acquisitions or a limitation of the aerosol to propagate to that area of the lung, despite normal lung ventilation, that appeared to be depicted on the 4DCT.

3.B. Dice similarity coefficients (DSC)

Table I reports the DSCs obtained between the high and low ventilation function volumes derived from the CT-ventilation maps and those extracted from corresponding SPECT-V images. For all six patients, the DSC of the high function volume was higher when derived from the stress map than from the Jacobian or change in HU, and the mean was significantly higher ($P < 0.01$). For the low function volumes, the stress maps yielded the highest DSC for all but two patients (4 and 6). The DSC values for the low function volumes obtained with the stress maps were significantly higher than with the Jacobian ($P < 0.01$) but not higher than those obtained with the change in HU ($P = 0.12$), an effect that was mostly due to the differences observed for Patient 4.

Patients 5 and 6, who presented the highest Spearman correlation coefficients between the stress map and SPECT-V, also presented the highest DSC between corresponding functional volumes. Figure 5 represents the low and high function volumes for those two patients who presented two different kinds of defects. Patient 5 exhibited emphysema in the superior parts of both lungs. Because of the resulting low HU values, the biomechanical model assigned

a low elasticity in this area, leading to low stress values. Patient 6 exhibited relatively normal tissues across the whole lung but the disease prevented the aeration of the middle and superior lobes of the right lung, leading to the absence of motion estimated by the biomechanical DIR and so to low stress values. The highest ventilation function areas given by the SPECT-V images were found for these two patients in the rest of the lung where the vasculature density was high. As a consequence of defining these areas as stiffer in the biomechanical model, the stress map showed consistently high values.

4. DISCUSSION

In terms of correlation with SPECT-V images, the method outperformed other methods based on the computation of the Jacobian determinant or changes in HU alone. The stress maps presented the highest correlation with SPECT for all of the six patients analyzed but one, for whom the HU-change method performed better. For the methods based on the Jacobian or changes in HU, other DIR algorithms may potentially yield to a higher correlation but the Spearman coefficients obtained in this study, with mean values of 0.39 ± 13 and 0.37 ± 18 respectively, were similar with the highest coefficients previously reported. A case scenario for which the Jacobian determinant alone was likely to present a poor correlation with reference ventilation imaging is when bullae or emphysema were present in the lung as it has been illustrated previously[29] and in this study. Volume expansions were indeed still occurring in these areas following inspiration despite the absence of lung function. The inverse of the DVF was used for the determinant of the Jacobian and no constraint in this algorithm ensured inverse consistency in the DVF which may be a limitation in this calculation. The interpretation of the performance of the HU changes-based method is more challenging. One drawback of this HU-based method could be a higher sensitivity to image artifacts, which are common with 4DCT imaging and can lead locally to a completely wrong estimation of the intensity. By using only contours of the lung and autosegmentation of the vasculature to estimate the deformation, Morfeus is probably less sensitive to these motion artifacts than global intensity-based DIR methods, but the estimated CT-ventilation metrics could still be impacted.

The V_{Jac} and V_{HU} maps computed in this study were implemented to serve as a baseline as they correspond to the most commonly used CT-ventilation imaging metrics. Variants or combinations of these metrics may lead to a stronger correlation. However, the results reported in this paper are consistent with those recently reported for other datasets and other ventilation imaging modalities in the context of the VAMPIRE Challenge.[22] The proposed algorithm performed the best for the two validation datasets of human subjects, one of 20 PET-Galligas and one of 11 DTPA-SPECT, with mean Spearman correlation coefficients of 0.53 ± 0.10 and 0.49 ± 16, respectively.

Uncertainties with the proposed biomechanical model-based method may come from the assumption of a linear relationship between the local density of the tissue in the CT scans and the stiffness. The choice of the Young's modulus range was empirical. However, since variations in the Young's modulus had little impact on the strain estimation and since ventilation maps are intended to provide relative and not absolute values of the ventilation function, the choice of this range does not matter as long as it ensures a linear relationship

between the stress and strain. To ensure a smooth distribution of the elasticity in the FEM, the Young's moduli assigned to the mesh nodes were based on a Gaussian smoothing of the CT image. Without this type of filtering, mesh nodes located close to but outside of vessels could be assigned low Young's moduli and the model could underestimate the local stiffness. The optimal radius of the Gaussian filter is directly related to the resolution of the FEM, with finer meshes which capture more anatomical information requiring smaller image smoothing. These two parameters were chosen empirically in this study and their optimal value will be optimized in future work based on a larger cohort of patients.

No consensus exists regarding the minimum required Spearman correlation coefficient to indicate that a CT-ventilation map is considered a good surrogate to the reference ventilation image. In a study comparing radiotherapy plans optimized using either SPECT or CT-ventilation maps for functional lung avoidance, the authors found that when the Spearman coefficient between the two ventilation maps was on the order of 0.4, a reasonable agreement was observed between the final functional lung sparing planned dose distributions.[30] For all patients in this study with the exception of Patient 4, the Spearman correlation coefficient between the stress map and SPECT-V image was consistently >0.5, suggesting the proposed method could serve as a good surrogate for SPECT-V for treatment planning purposes. Achieving a higher correlation might be possible, especially considering recent advances in deep learning techniques, but without necessarily being more clinically relevant for current models of functional sparing in treatment planning. Existing ventilation mapping methods are indeed known to be associated with uncertainties and artifacts. Especially, while it was not the case for the six patients analyzed in this study, SPECT-V image quality commonly suffers from clumping of the aerosol in the airways.[31] The mechanistic approach proposed in this study may provide a more reliable mapping of the actual ventilation function.

5. CONCLUSION

This paper describes an original approach to generate lung ventilation function images through stress maps derived from biomechanical model-based DIR. The generated ventilation maps presented a significantly stronger and more consistent correlation with standard SPECT-V images than previously proposed CT-ventilation metrics did. We believe this approach is a very promising tool for incorporation in functional lung avoidance strategies.

ACKNOWLEDGMENTS

This work was funded in part by NIH P01CA059827.

CONFLICTS OF INTEREST

Kristy Brock received funding from RaySearch Laboratories AB through a Co-Development and Collaboration Agreement. Kristy Brock has a licensing agreement with RaySearch Laboratories AB. Martha Matuszak received research and consulting funding from Varian Medical Systems. Shruti Jolly is a consultant for Varian Medical Systems and AstraZeneca.

REFERENCES

1. Tyldesley S, Boyd C, Schulze K, Walker H, Mackillop WJ. Estimating the need for radiotherapy for lung cancer: an evidence-based, epidemio-logic approach. Int J Radiat Oncol Biol Phys. 2001;49:973–985. [PubMed: 11240238]
2. Sura S, Gupta V, Yorke E, Jackson A, Amols H, Rosenzweig KE. Intensity-modulated radiation therapy (IMRT) for inoperable non-small cell lung cancer: the Memorial Sloan-Kettering Cancer Center (MSKCC) experience. Radiother Oncol. 2008;87:17–23. [PubMed: 18343515]
3. Yamashita H, Takahashi W, Haga A, Nakagawa K. Radiation pneumonitis after stereotactic radiation therapy for lung cancer. World J Radiol. 2014;6:708–715. [PubMed: 25276313]
4. Marks LB, Bentzen SM, Deasy JO, et al.Radiation dose–volume effects in the lung. Int J Radiat Oncol Biol Phys. 2010;76:S70–S76. [PubMed: 20171521]
5. Yom SS, Liao Z, Liu HH, et al.Initial evaluation of treatment-related pneumonitis in advanced-stage non–small-cell lung cancer patients treated with concurrent chemotherapy and intensity-modulated radiotherapy. Int J Radiat Oncol Biol Phys. 2007;68:94–102. [PubMed: 17321067]
6. Rodrigues G, Lock M, D'Souza D, Yu E, Van Dyk J. Prediction of radiation pneumonitis by dose–volume histogram parameters in lung cancer —a systematic review. Radiother Oncol. 2004;71:127–138. [PubMed: 15110445]
7. Marks LB, Spencer DP, Sherouse GW, et al.The role of three dimensional functional lung imaging in radiation treatment planning: the functional dose-volume histogram. Int J Radiat Oncol Biol Phys. 1995;33:65–75. [PubMed: 7642433]
8. Siva S, Thomas R, Callahan J, et al.High-resolution pulmonary ventilation and perfusion PET/CT allows for functionally adapted intensity modulated radiotherapy in lung cancer. Radiother Oncol. 2015;115:157–162. [PubMed: 25935743]
9. Eslick EM, Stevens MJ, Bailey DL. SPECT V/Q in lung cancer radiotherapy planning. Semin Nucl Med. 2019;49:31–36. [PubMed: 30545514]
10. Guerrero T, Sanders K, Noyola-Martinez J, et al.Quantification of regional ventilation from treatment planning CT. Int J Radiat Oncol Biol Phys. 2005;62:630–634. [PubMed: 15936537]
11. Reinhardt JM, Ding K, Cao K, Christensen GE, Hoffman EA, Bodas SV. Registration-based estimates of local lung tissue expansion compared to xenon CT measures of specific ventilation. Med Image Anal. 2008;12:752–763. [PubMed: 18501665]
12. Castillo R, Castillo E, Martinez J, Guerrero T. Ventilation from four-dimensional computed tomography: density versus Jacobian methods. Phys Med Biol. 2010;55:4661–4685. [PubMed: 20671351]
13. Castillo R, Castillo E, McCurdy M, et al.Spatial correspondence of 4D CT ventilation and SPECT pulmonary perfusion defects in patients with malignant airway stenosis. Phys Med Biol. 2012;57:1855–1871. [PubMed: 22411124]
14. Hegi-Johnson F, Keall P, Barber J, Bui C, Kipritidis J. Evaluating the accuracy of 4D-CT ventilation imaging: first comparison with Technegas SPECT ventilation. Med Phys. 2017;44:4045–4055. [PubMed: 28477378]
15. Yamamoto T, Kabus S, Lorenz C, et al.Pulmonary ventilation imaging based on 4-dimensional computed tomography: comparison with pulmonary function tests and SPECT ventilation images. Int J Radiat Oncol Biol Phys. 2014;90:414–422. [PubMed: 25104070]
16. Fuld MK, Easley RB, Saba OI, et al.CT-measured regional specific volume change reflects regional ventilation in supine sheep. J Appl Physiol. 2008;104:1177–1184. [PubMed: 18258804]
17. Ding K, Cao K, Fuld MK, et al.Comparison of image registration based measures of regional lung ventilation from dynamic spiral CT with Xe-CT. Med Phys. 2012;39:5084–5098. [PubMed: 22894434]
18. Mathew L, Wheatley A, Castillo R, et al.Hyperpolarized 3He magnetic resonance imaging: comparison with four-dimensional x-ray computed tomography imaging in lung cancer. Acad Radiol. 2012;19:1546–1553. [PubMed: 22999648]
19. Kipritidis J, Siva S, Hofman MS, Callahan J, Hicks RJ, Keall PJ. Validating and improving CT ventilation imaging by correlating with ventilation 4D-PET/CT using 68Ga-labeled nanoparticles. Med Phys. 2014;41:011910. [PubMed: 24387518]

20. Yamamoto T, Kabus S, von Berg J, et al.Evaluation of four-dimensional (4D) computed tomography (CT) pulmonary ventilation imaging by comparison with single photon emission computed tomography (SPECT) scans for a lung cancer patient. Paper presented at: Proceedings of the Third International Workshop on Pulmonary Image Analysis; 2010.
21. Cazoulat G, Owen D, Matuszak MM, Balter JM, Brock KK. Biomechanical deformable image registration of longitudinal lung CT images using vessel information. Phys Med Biol. 2016;61:4826. [PubMed: 27273115]
22. Kipritidis J, Tahir BA, Cazoulat G, et al.The VAMPIRE challenge: aa multi-institutional validation study of CT ventilation imaging. Med Phys. 2019;46:1198–1217. [PubMed: 30575051]
23. Al-Mayah A, Moseley J, Velec M, Brock KK. Sliding characteristic and material compressibility of human lung: parametric study and verification. Med Phys. 2009;36:4625–4633. [PubMed: 19928094]
24. Al-Mayah A, Moseley J, Velec M, Hunter S, Brock K. Deformable image registration of heterogeneous human lung incorporating the bronchial tree. Med Phys. 2010;37:4560–4571. [PubMed: 20964173]
25. Sundaram TA, Gee JC. Towards a model of lung biomechanics: pulmonary kinematics via registration of serial lung images. Med Image Anal. 2005;9:524–537. [PubMed: 15896996]
26. Zhang T, Orton NP, Mackie TR, Paliwal BR. A novel boundary condition using contact elements for finite element based deformable image registration. Med Phys. 2004;31:2412–2415. [PubMed: 15487720]
27. Al-Mayah A, Moseley J, Brock K. Contact surface and material nonlinearity modeling of human lungs. Phys Med Biol. 2007;53:305. [PubMed: 18182705]
28. Villard P-F, Beuve M, Shariat B, Baudet V, Jaillet F. Simulation of lung behaviour with finite elements: Influence of bio-mechanical parameters. Paper presented at: Third International Conference on Medical Information Visualisation--BioMedical Visualisation; 2005.
29. Kipritidis J, Hofman MS, Siva S, et al.Estimating lung ventilation directly from 4D CT Hounsfield unit values. Med Phys. 2016;43:33–43. [PubMed: 26745897]
30. Kida S, Bal M, Kabus S, et al.CT ventilation functional image-based IMRT treatment plans are comparable to SPECT ventilation functional image-based plans. Radiother Oncol. 2016;118:521–527. [PubMed: 26922488]
31. Schembri GP, Roach PJ, Bailey DL, Freeman L. Artifacts and anatomical variants affecting ventilation and perfusion lung imaging. Semin Nucl Med. 2015;45:373–391. [PubMed: 26278851]

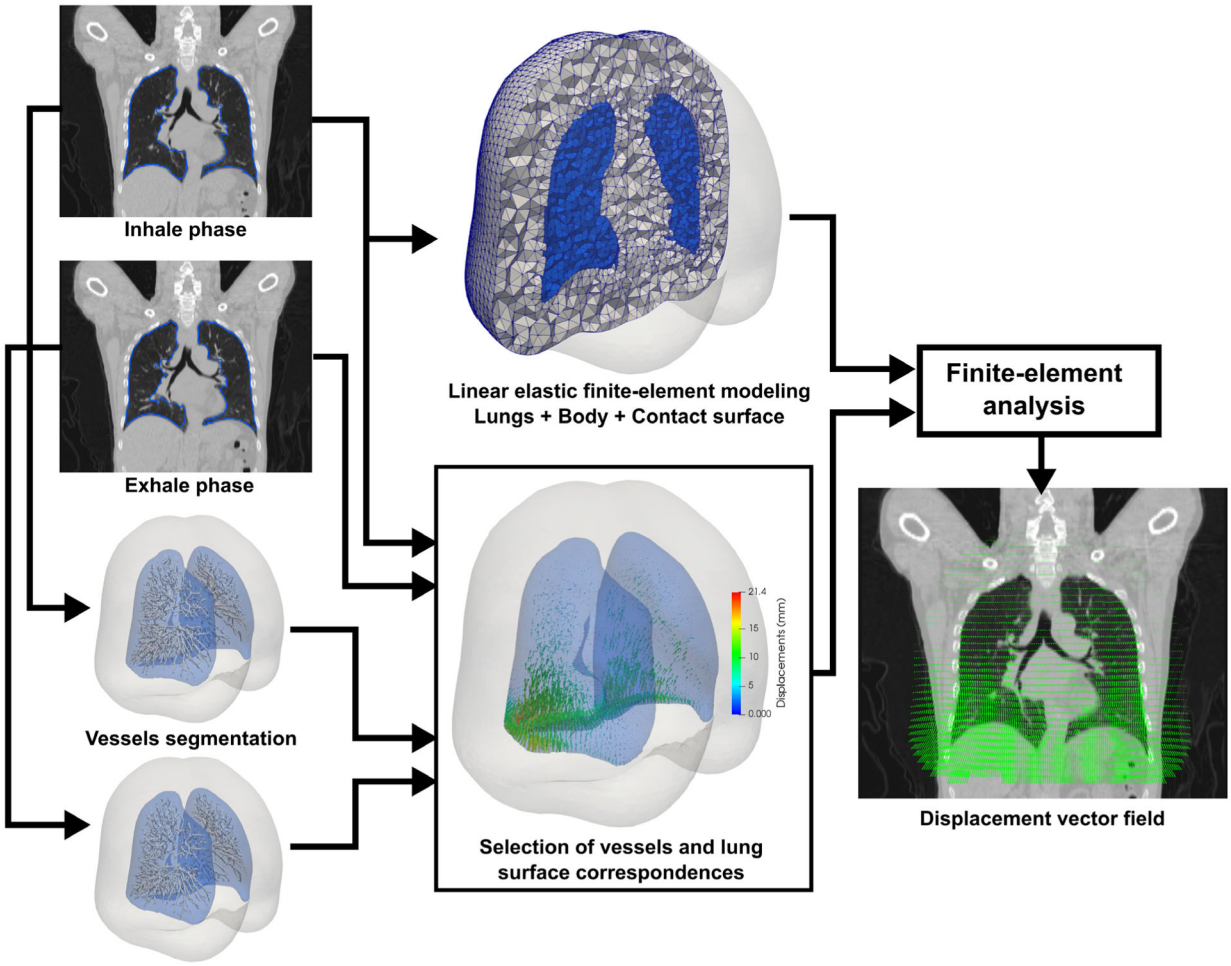

FIG. 1.

Morfeus workflow for the deformable image registration between the inhale and exhale phases of a four-dimensional computed tomography scan.

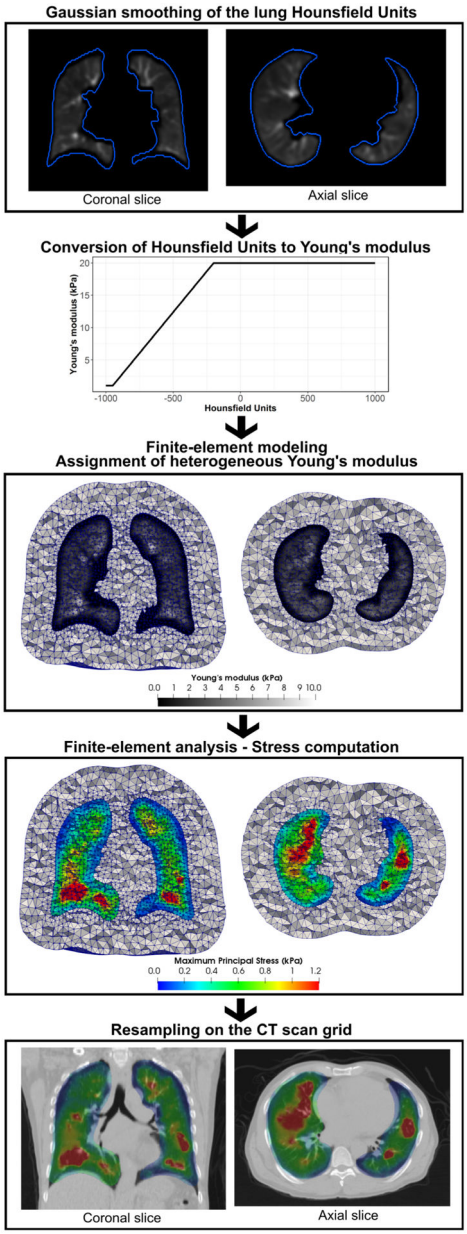

FIG. 2.

Expansion of the Morfeus method workflow described in Fig. 1 for the generation of stress maps.

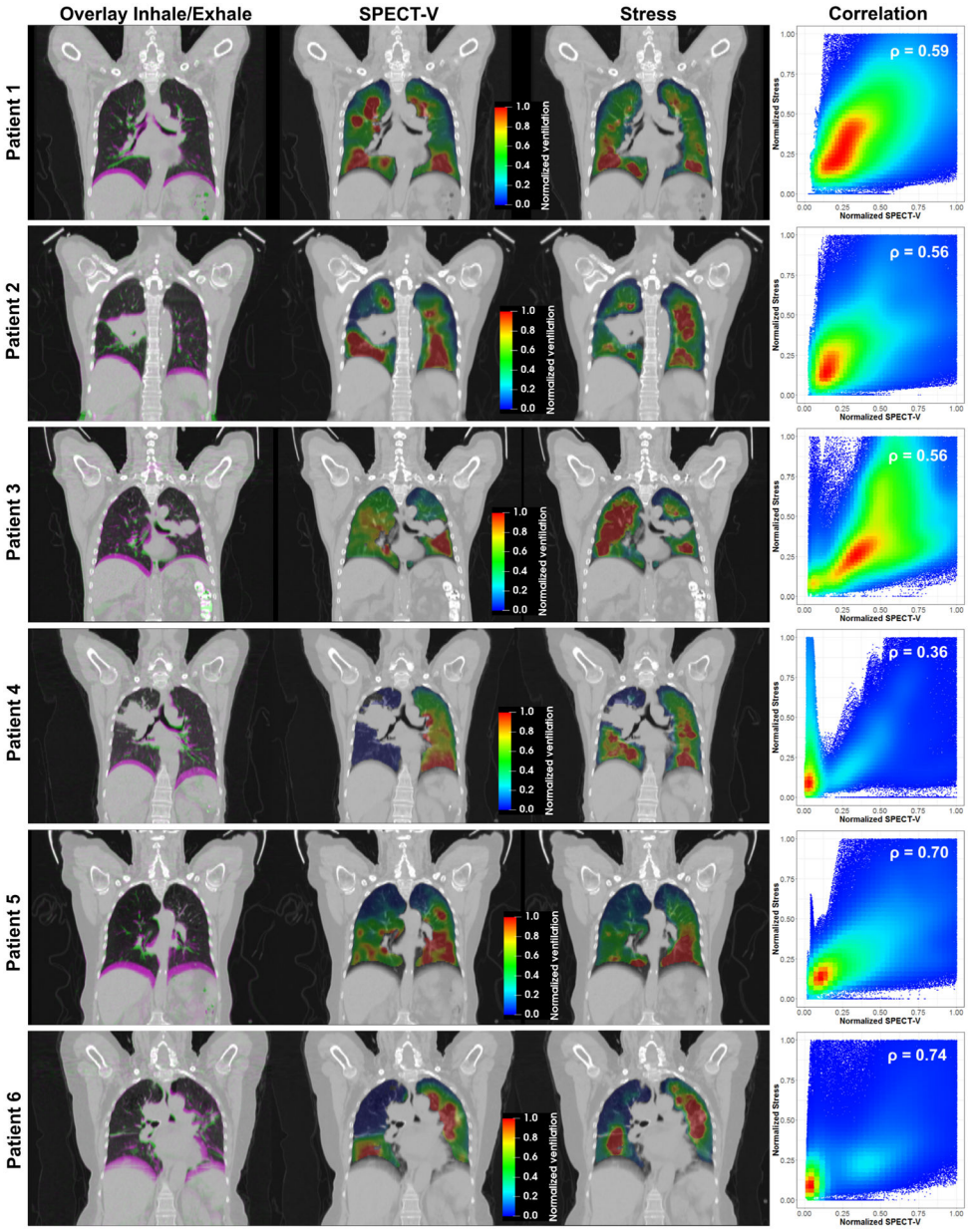

FIG. 3.

Illustration of the breathing magnitude between the inhale and exhale phases of the four-dimensional computed tomography and of the correlation between the reference SPECT-V images and computationally generated stress maps.

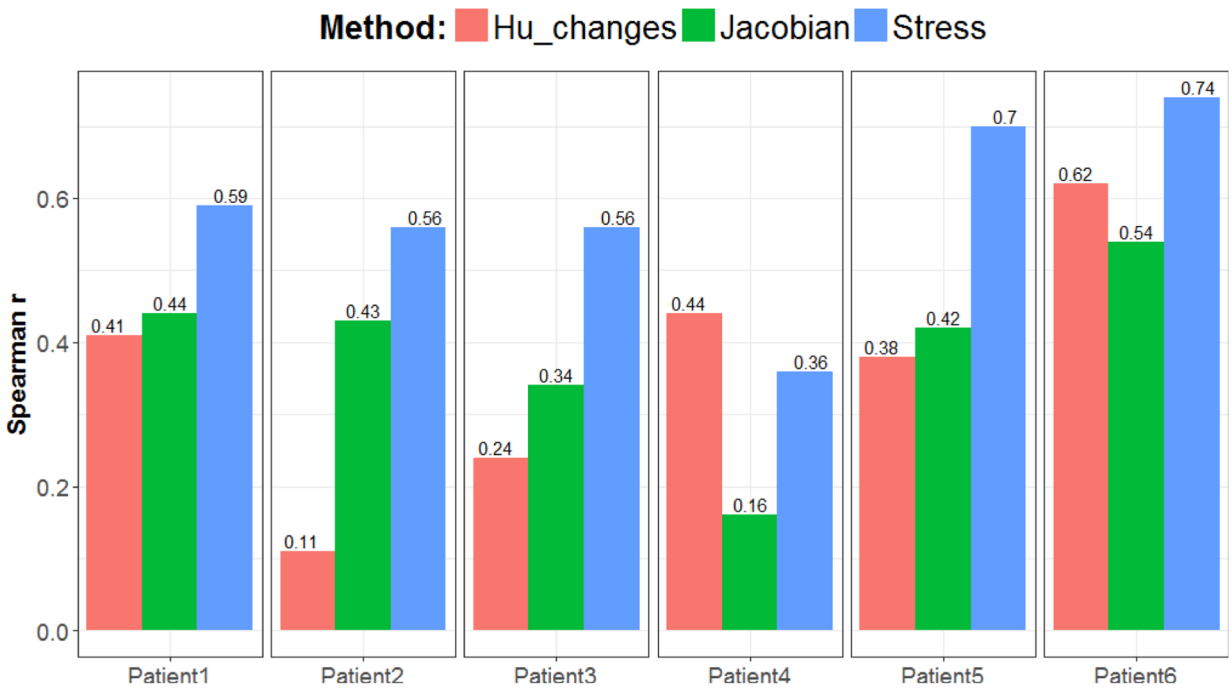

FIG. 4.

Spearman correlation coefficients between each computed tomography-ventilation metric and the reference SPECT-V for the six patients.

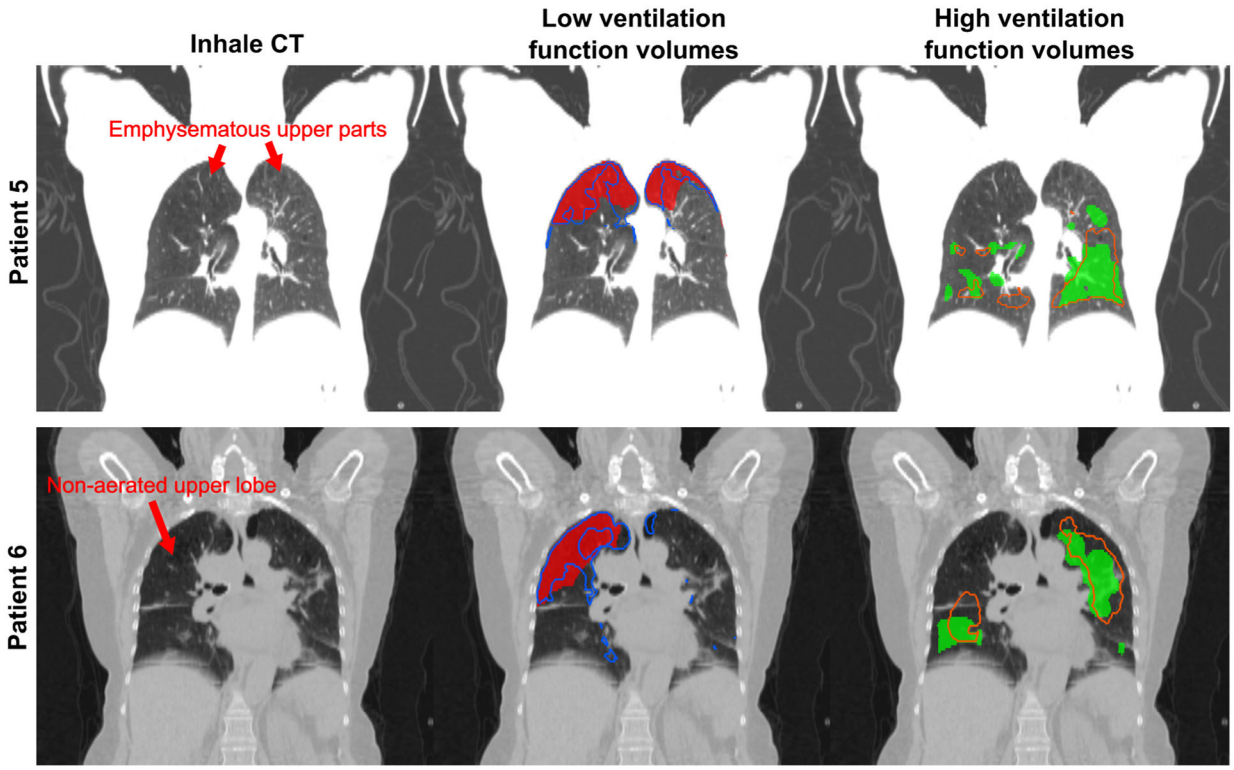

FIG. 5.

Representation for the two patients presenting the highest correlation between stress maps and reference SPECT-V images of the low and high function volumes obtained by thresholding. The plain red and green area represent respectively the low and high function volumes derived from the SPECT-V. The blue and orange contours represent the same volumes but derived from the stress maps.

TABLE I.

Dice similarity coefficients between ventilation function volumes from CT-ventilation maps and reference SPECT-V images.

	Low function volume DSC			High function volume DSC		
	Stress	**Jacobian**	**HU**	**Stress**	**Jacobian**	**HU**
Patient1	**0.55**	0.49	0.48	**0.52**	0.43	0.40
Patient2	**0.52**	0.31	0.33	**0.46**	0.24	0.29
Patient3	**0.65**	0.49	0.47	**0.42**	0.35	0.28
Patient4	0.39	0.36	**0.46**	**0.52**	0.36	0.50
Patient5	**0.66**	0.43	0.41	**0.57**	0.44	0.45
Patient6	0.69	0.55	**0.72**	**0.60**	0.40	0.34
Mean	**0.58**	0.44	0.48	**0.52**	0.37	0.38
STD	0.11	0.09	0.13	0.07	0.07	0.09

For each patient, the highest low function volume DSC and highest high function volume DSC are indicated in bold.